Residual flow patterns and morphological changes along a macro- and meso-tidal coastline

Nicoletta Leonardi[1], and Andrew James Plater[1]

[1]Department of Geography and Planning, School of Environmental Sciences, University of Liverpool, Roxby Building, Chatham St., Liverpool L69 7ZT, UK

Abstract

The hydrodynamic and residual transport patterns arising from oscillating tidal motion have important consequences for the transport of sediments, and for the evolution of the shoreline, especially under macro- and meso-tidal conditions. For many locations there are significant uncertainties about residual currents and sediment transport characteristics, and their possible influence on the morphological evolution of the coastline and on the character of the bed. Herein we use the coastline of SE England as a test case to investigate possible changes in residual currents, and residual transport patterns from neap to spring tide, the reciprocal interaction between residuals and the character of the bed, and the morphological evolution of the coastline at a century timescale. We found that in the long term the morphology of the system evolves toward a dynamic equilibrium configuration characterized by smaller, and spatially constant residual transport patterns. While the spatial distribution of residual currents maintains a similar trend during both neap and spring tide, during spring tide and for large areas residual currents switch between northerly and southerly directions, and their magnitude is doubled. Residual eddies develop in regions characterized by the presence of sand bars due to the interaction of the tide with the varying topography. Residual transport patterns are also computed for various sediment fractions, and based on the hydrodynamics and sediment availability at the bottom. We found that the distribution of sediments on the bed is significantly correlated with the intensity of residuals. Finally, the majority of long-

term morphological changes tend to develop or augment sand banks features, with an increase in elevation and steepening of the bank contours.

Introduction

Tidal dynamics and residual circulation are important for the fate and transport of sediments, contaminants, and potentially have important consequences for the morphodynamic evolution of the coastline. The coastline of SE England is a region of enormous importance from an economic point of view; and due to the natural alternation of different shoreline types, such as saltmarsh, soft cliff and sand dunes, it is also unusual from an environmental and tourist standpoint (e.g. Schans et al., 2001). Understanding the physical processes acting along these shorelines is fundamental for a correct management of the ecosystem, and to determine the impact of human activities and climate change upon them (e.g. Schans et al., 2001; Androsov et al., 2002; Robinson et al., 2007; Liang et al., 2013; Brooks and Spencer, 2014; Armstrong et al., 2015; Hackney et al., 2015; Brooks et al., 2017).

Using a hydrodynamic and morphological model, this paper aims to explore residual transport patterns for the coastline of SE England, as well as possible long-term morphological changes in the area. Even though this coast has been the subject of several insightful studies (e.g. Horillo-Caraballo and Reeve, 2008; Dyer and Moffat, 1992; Robinson, 1965; Dyer, and Huntley, 1999), our understanding of residual transport and sediment distribution patterns remains unclear. The majority of existing studies are based on relatively large scale and coarse-resolution models developed at the scale of the North Sea rather than at a coastline scale, and in terms of field measurements some classic limitations are present which are connected to the fact that, even in case of extensive field campaigns, only a discrete number of measurements can be collected and a compromise between spatial or temporal resolution need to be found. Furthermore, for the area of interest, some existing

51 modelling studies have focused mainly on the hydrodynamics of the system and have
52 neglected the resuspension of sediments at the bottom, and tide-induced morphological
53 changes (e.g. Chini et al., 2010; Stanev et al., 2009).
54 Along coastal environments tides can interact with the variable bathymetry and a complex
55 residual flow can be created due to varying topography, bottom friction, and tidal
56 asymmetries (e.g. Brown et al., 2014; Brown and Davies, 2010). Eulerian residual currents
57 are defined as the velocity at a fixed location, and averaged over multiple tidal cycles. These
58 second-order currents, driven by non-linear tidal dynamics, have been recognized as a
59 significant component of the flow field, and can be relevant to sediment dynamics (e.g.
60 Burchard and Hetland, 2010; Iannelolo et al, 1979; Nihou and Rodnay, 1975; Zimmermann,
61 1981; Leonardi et al., 2013, 2015). Embedded within the southeast part of the North Sea, the
62 large-scale residual circulation of the area has been studied for a long time: the southern
63 portion of the Suffolk and Essex coastline is characterized by northwest directed surface
64 currents coming from the English Channel, while the northern portion is partially affected by
65 the large anticlockwise gyre generated by the North Atlantic mixing water (e.g. Mathis et al.,
66 2015; Svendsen et al., 1991; Winther and Johannessen, 2006). Residual currents can be also
67 explained in terms of vorticity transfer from the oscillating to the average flow field: for a
68 non-vanishing residual circulation there needs to be some vorticity production as well as a net
69 flux of vorticity over a closed boundary and over a tidal cycle. In the case of topographic
70 features such as sand ridges, by considering a closed line around the ridge there is a net influx
71 of clockwise vorticity (or outflux or anti-clockwise), generated by the torque induced by both
72 Coriolis and frictional forces which are stronger on the shallower than on the deeper side, and
73 which creates residual eddies (Zimmermann, 1981).
74 This paper is organized as follows: a general description of the study area is provided,
75 followed by a methodology section illustrating the numerical model set-up. The results

section is organized into two main parts: an initial part dealing with the main features of the system in terms of hydrodynamics and residual currents, and a second part dealing with sediment transport patterns and morphological changes. A set of discussions and conclusions is finally presented.

Study site

The coastline of SE England is of great importance from a social and ecological point of view, and it is characterized by a variety of shorelines, from sandy beaches, saltmarshes, shingle banks and soft cliffs (cf. Schans et al., 2001). The northeast portion of the coastline is characterized by soft chalk cliffs, which dip seaward and go below mean sea level near Sheringham where the chalk is succeeded by Tertiary deposits covered by glacial beds. North Norfolk is characterized by both back-barrier and open coast saltmarshes, with low angle sand flats (Steers et al., 1926; Moeller et al., 1999). The marshland comes to an end at Weybourn, and from there until the Thurne River, the area becomes characterized by soft cliffs of varying height, which are subject to erosion processes. The coastline is interrupted by large cuspate projections, i.e. 'nesses', representing depositional features largely built of sand, rather than originating from more resistant rocks. Sandbanks are common in the North Sea as well. Following the classification proposed by Dyer and Huntley (1999), the Norfolk coastline is characterized by headland associated banks in the form of alternating ridges with recessional headlands (type 3B according to the classification); the Suffolk coastline is instead characterized by banner banks related to non-recessional banks (type 3A). The mouth of the Thames comprises wide mouth ridges (type 2A), and the area immediately south of the Thames is characterized by both alternating ridges with recessional headlands, and banner banks. South of the Thames, several others shoreline features alternate, i.e. narrow sand and shell beaches around the Isle of Grain, pocket beaches or sandstone cliffs around Thanet and

Dover districts, gravel beaches around Dungeness. The entire SE England coast is also characterized by large human interventions, and hard engineering structures such as seawalls or groins are present.

The tides in the North Sea are mainly semi-diurnal, and progress anticlockwise, with the largest amplitudes present along the eastern England and German Bight coasts (Huthnance, 1991). The tidal range for the SE England coasts varies from meso- to macro-tidal, and both tidal range and tidal phase vary significantly along the area due to vicinity with North-Sea amphidromic systems (Figure 1A). Within the area of interest several turbidity studies have identified offshore locations with high sediment concentration: the East Anglian plume. This plume is more pronounced in winter, and the highest concentrations occur around the Norfolk banks (e.g. Dyer and Moffat, 1998). For the coastline as a whole, the fluvial sediment supply is generally considered negligible (e.g. McCave, 1987). For the North Sea in general, sediment supplies include the ones coming from the North Atlantic and from the English Channel (quantified as $10x10^6$ ta^{-1}), and from seafloor erosion ($6\text{-}7.5x10^6$ ta^{-1}). A contribution to suspended sediments can also come from the erosion of Norfolk cliffs ($6.65\ x10^5$ ta^{-1}). Due to difficulties in closing the sediment budget, large uncertainties of around ± 50% characterize these estimates of sediment budget (Dyer and Moffat, 1995; McCave, 1987).

Methods

Herein we use the computational fluid dynamics package Delft3D (e.g. Lesser et al., 2004). Delft3D is made of a number of integrated modules allowing the coupled simulation of hydrodynamic, sediment transport and morphological processes. The Delft3D-FLOW module constitutes the package core and solves the unsteady shallow water equations, following the Boussinesq approximation. The vertical momentum equation is reduced to the hydrostatic pressure relation because vertical accelerations are assumed to be small compared to the gravitational one (Lesser et al., 2004).

126 The model is here used in 2D depth averaged mode with Delft3D default eddy diffusivity
127 value, equal to 10 m^2/s. The model accounts for wetting and drying of areas which are not
128 permanently under water. For more details about the hydrodynamic module we refer to
129 (Lesser et al., 2004).
130 Sediment transport and morphology modules support both non-cohesive, and cohesive
131 sediment fractions, and both bed-load and suspended load. In case of cohesive sediments, the
132 Partheniades–Krone formulation is used: the erosive flux is modelled as proportional to an
133 erosion parameter, and to a Heaviside function which depends on the exceedance shear stress
134 with respect to a critical shear stress for erosion (Partheniades 1965); the depositional flux is
135 given by bottom concentration per settling velocity values (Winterwerp 2007). In the original
136 Partheniades 1965 formulation, the critical shear stress for erosion is always greater than or
137 equal to the one for deposition; therefore, intermediate shear-stress conditions may exist for
138 which neither erosion nor deposition occurs. This is in contrast to common observations and
139 assumptions for non-cohesive sediments, according to which deposition and erosion always
140 occur simultaneously (Sanford and Halka 1993). Winterwerp (2007) more recently reviewed
141 the cohesive-sediment paradigm by means of literature data, and concluded that the so-called
142 critical shear stress for deposition does not exist, but is simply a threshold for resuspension.
143 The latter consideration was also postulated by Krone in his original report (Krone 1962).
144 These findings are in agreement with observations of Sanford and Halka (1993) in the upper
145 Chesapeake Bay. Therefore, we choose to assume a gross sedimentation rate of cohesive
146 sediments equal to their settling flux, which is the approach recommended for the used
147 numerical framework (Winterwerp 2007). For the transport of non-cohesive sediments we
148 followed the default formulation, i.e. Van Rijn et al., 2003, 2004. The erosive flux of
149 sediments is proportional to the following: i) a vertical sediment mixing coefficient, ii) the
150 concentration gradient along the vertical. The mixing coefficient depends on a factor (β)

proportional to: i) settling velocity, ii) critical shear velocity at the bottom (Van Rijn, 1984). The concentrations at the bottom, and concentration gradient are calculated following a standard Rouse profile which starts from a reference height, a, and concentration, c_a. The deposition flux is proportional to the concentration and settling velocity. The reference height, concentration, and settling velocity are calculated following Van Rijn 1993 (Van Rijn 1993; Hydraulics, D., 2014). For more information about the numerical model specifications in regard to sediment transport we also refer to Hydraulics, D., 2014.

Bathymetry data are based on tiles with size 30x30 m of the product Arcsecond Gridded Bathymetry (ASC geospatial data), retrieved from the EDINA Marine Digimap download service (http://digimap.edina.ac.uk/). For areas covering the shoreline, DTM data from LiDAR surveys at 2 m resolution were used, which were downloaded from the UK Environment Agency's LiDAR data archive. Bathymetric data were referred to Lowest Astronomical Tide and LiDAR data to Ordnance Datum, and spatially varying Vertical Offshore Reference Frame (VORF) corrections as provided by the UK Hydrographic Office were applied.

Sediment transport and morphology modules in Delft3D allow accounting for multiple sediment fractions. The transport of each sediment class is separately calculated taking into account the availability of each fraction in the bed. The erodible bed is divided into 3 vertically mixed layers (one base layer, one under layer, and a transport layer). A minimum of three layers is required to have a spatially varying sediment distribution in the model. The thickness of the transport layer is 0.1 m. At every time step the exposed layer (the transport layer) is the one providing sediments to the flow, and for every time step layers thickness is updated. If the thickness of the transport layer exceeds 0.1 m, the exceedance is incorporated into the under layer; however, if the transport layer is eroded, the latter is replenished from the under-layer. The total initial bed thickness is around 300 m to be sure to avoid to exceed

sediments availability trough scour. The under layer is 100m, and the base layer 200m. The number of layers was limited to three due to computational reasons. The input for the initial spatial distribution of sediments at the bottom (constant across the three layers) was created starting from the British Geological Survey (BGS) GIS-maps for seabed sediments and parent material (near-surface geology) for the more landward side of the domain (Figure 2). BGS datasets provide detailed information with regard to Lithology, Texture, Mineralogy (and others), and in this regard sediment types are divided into numerous classes. In relation to the number of grain classes used in the computation, the dataset was simplified and reduced to four main sediment classes, i.e. sand, gravel, mud, rock. Standard settling velocities, median grain diameters and critical shear strength values were attributed to each sediment class. Sand and gravel sediment diameter is set equal to 200 µm for sand, and 2000 µm for gravel, and the critical shear stress for erosion for mud is set constant and equal to 0.5 $N/m^{2,}$ and the erosion parameter equal to 0.0001 $kg/m^2/s$ as default. Figure 2 illustrates the distribution of sediments within the domain; sand is the most abundant fraction, especially for more offshore areas, but gravel is present as well and gravel-sand mixtures characterize a great part of the coastline, while the mud fraction is mostly present within the Thames estuary.

The model is divided into two separate domains (Figure 1b, c) which are fully coupled through the domain decomposition option, and exchange information along internal boundaries. Domain decomposition methods are techniques for solving partial differential equations based on a decomposition of the spatial domain of the problem into several subdomains whose computations are carried out concurrently. Domain decomposition allows local grid refinement (e.g. Chan et al., 1994; Hydraulics, D., 2014). The domain decomposition option was adopted to maximize the spatial resolution along part of the coastline without compromising the computational time. Average grid cell size for the exterior domain is 1500 x 500 m, and for the smaller domain is 400 x 200 m.

Simulations are run from June 2008 to July 2009. Results are mainly presented in relation to the highest spring tide (11 February 2009), and lowest neap tide (8 October, 2008) of the simulation period. When taking the morphological evolution into account a morphological scale factor, *n*, of 100 is considered. This factor simply increases the incremental depth changes at each time step by a constant *n*, so that after simulating one tidal cycle, the simulation is actually representative of the morphological changes which are expected to happen after *n* cycles; this is similar to the concept of elongated tide proposed by Latteux (1995). According to the lengthening of the tide concept of Latteux, 1995, N successive tides can be simulated by a single one extended N times, i.e. by lumping together successive tidal cycles after computing the hydrodynamic at a proper time scale. As the hydrodynamic vary much more slowly than the morphology, the longer time step obtained by combining the N cycles is such that after this time, the evolution of the bed is not negligible anymore, and bed level and flow conditions are adjusted accordingly.

Exterior boundary conditions are provided by the Extended Area Continental Shelf Model fine grid (CS3X) which has 1/9° latitude by 1/6° longitude (approximately 12 km) resolution, and covers areas from 40° 07'N to 62° 53' N, and from 19° 50'W to 12° 50'E. The CS3X model makes use of meteorological data from the UK Met Office Operational Storm Surge model. Pressure and wind input data for the Delft3D model were generated from the same UK Met Office model; the resolution of wind and pressure data are based on two different computational grids having size of approximately 12, and 48 km respectively. The boundary conditions for Delft3D were provided every hour. Hourly water level data from different buoys for the calibration of the Delft3D model were retrieved from the British Oceanographic Data Centre (https://www.bodc.ac.uk/data/online_delivery/ntslf/processed/).

The accuracy of the spatial distribution of water elevation was evaluated following classical harmonic analysis, and Skill Score values based on root mean square error and standard

deviation values. Specifically, we used the Brier Skill Score (Murphy and Epstein, 1989) defined as:

$$BSS = \frac{\alpha - \beta - \gamma + \varepsilon}{1 + \varepsilon}$$

where $\alpha = r_{XY}^2$, $\beta = \left(r_{XY} - \frac{\sigma_Y}{\sigma_X}\right)^2$, $\gamma = \left(\frac{\langle Y \rangle - \langle X \rangle}{\sigma_X}\right)^2$, $\varepsilon = \left(\frac{\langle X \rangle}{\sigma_X}\right)^2$ for which r is the correlation coefficient, σ is the standard deviation, ε is a normalization term, and X and Y are observed and model values. The skill class was assumed to be excellent for BSS in the interval 1-0.65, very good for 0.65–0.5, good for 0.5–0.2, and poor for 0.2-0, based on the related literature (e.g. Allen et al. 2007; Ralston et al. 2010; Sutherland et al. 2004; Zafer and Ganju, 2014).

Results

A comparison between modelled tidal elevations and buoy data is presented in Figure 3 (and Figure S1), for 5 buoy stations (site locations in Figure 1b). Modelled tidal levels generally show good agreement with the instrumental data, and Brier Skill Scores are excellent with values ranging from 0.84 to 0.97. For visualization purposes, Figure 3 only shows values for 75 days of simulation time. We further conducted harmonic tidal analysis of both Delft3D, and buy data tidal constituents using T_Tide, an open source toolbox developed by Pawlowicz et al., 2002. The toolbox uses the least square error method to conduct classic harmonic analysis for periods less than one year, and by also using nodal corrections; results from the harmonic analysis are presented in table S1 according to which the model reproduces satisfactory results in terms of both tidal amplitude, and phase.

Figure 4 shows maximum bed shear stress values for the lowest neap tide (8 October, 2008; panel A, D), and highest spring tide (11 February 2009; panel B, E) of the run period. Maximum bed shear stress values during the spring tide reach 9.2 N/m^2, and are 2.6 times

249 larger than the maximum shear stress values during neap tide. Greatest differences in shear
250 stress between spring and neap tide occur around the areas of Lowestoft and Dover (panel C).

251 Figure 5 shows residual currents during neap tide (A, D, E), spring tide (B, F, G), and
252 differences in the two (C) for the exterior and inner domain. Residual currents and residual
253 transport patterns were calculated by averaging these over 5 tidal cycles, two tidal cycles
254 before and two after the lowest and highest neap and spring tidal cycles.

255 Several mechanisms contribute to the formation of tidal residual currents, which can be
256 decomposed into three main contributions (e.g. Burchard et al., 2010; Cheng et al., 2011): (1)
257 the density driven flow which depends on buoyancy gradient; (2) symmetrical tidal mixing,
258 which is connected to the correlation between eddy viscosity and vertical shear, and thus to
259 tidal straining, relevant to tidal asymmetry; and (3) vertically averaged tidal mean velocity,
260 connected to the residual riverine flow and to non-linear flow mechanisms related to the
261 various terms in the the De Saint–Venant equations, namely the non-linear frictional and
262 advective terms in the momentum equation (e.g. Parker, 1991; Tee 1977). Residual currents
263 calculated here are depth averaged, and are thus only representative of the third mechanism
264 described above. The presented residual currents maintain a similar pattern during spring and
265 neap tide (e.g., compare Figure 5A with 5B), but maximum spring values increase up to 54%
266 with respect to neap tide, and average residual values increase by 113%. The maximum
267 differences between the residual currents at spring and neap tide is 0.25 m/s. For the higher
268 resolution inner domain (panels D to G), the formation of classic gyre circulations around bar
269 axes is noteworthy. In fact, for a tidal flow oscillating along varying water depth contours
270 more friction is felt on the more gently sloping side, and a frictional torque is developed
271 (Pingree and Maddock, 1985; Zimmermann, 1981). Residual current magnitudes around sand
272 bars largely increase during spring tides. Residual currents are also visualized with respect to
273 bathymetry values to highlight the vorticity trend around the bars (Figure 5E, G). During both

neap and spring tides, channels areas are flood-dominated (residual currents directed South West) while intertidal mudflats are ebb-dominated (residual currents directed North East). During the spring tide the extent of flood-dominated areas largely increase (Figure 6E, to F). Even if residuals are higher during the spring tide, recirculating gyres are identifiable, and maintain the same organization during both spring and neap tide.

Figure 6 shows the angle of residual currents during neap (panel A, E) and spring tides (panel B, F), and corresponding frequency distribution of magnitude. During the neap tide, the direction of residual currents of the external domain is more uniformly distributed and mostly directly north-eastward, apart from the northern portion of the domain and channel areas within the Thames estuary. For these areas residuals are south-westerly and directed landward, while for the rest of the domain they are mostly directed seaward. During the spring tide, residual currents within the entire domain assume a bimodal distribution around 45 degrees and 250 degrees, indicating more southerly directed currents. Moreover, during spring tide large areas within the Thames transition from ebb to flood dominance, and a large portion of the system becomes flood-dominated. This can be also observed by looking at the frequency distribution of residual currents directions (compare panels C and D, and panels G and H).

Changes in the magnitude of residual currents from neap to spring tide are also presented as a function of the bed level (Figure 7, deepest areas to the left). Grey points refer to the entire domain, while blue points refer to the smaller, higher resolution domain. A significant relationship between the two variables (changes in residuals magnitude and bed level) can be found indicating that strongest changes in residual currents are typically found around the deepest areas. In contrast, no relationship could be found in between changes in residual current direction and water depth.

Sediment transport and morphology

The transport of sediments, as well as morphological changes, are dictated by both hydrodynamic conditions and sediments availability. Figure 8 shows the relationship between the initial percentage of the different sediment fractions at the bottom and the following variables: residual velocity values (Figure8, panels A to C), mean bottom shear stress (panels D to F), and maximum bottom shear stress (panels G to I) during spring tide. These three variables are the ones most commonly used for the description of the velocity field in tidally dominated environments. Correlation exists between mud availability and the intensity of residual currents, with the presence of mud decreasing with residual currents intensity. A similar inverse relationship can be found between mud availability and mean and maximum shear stress values. A positive correlation is instead present in case of gravel, and sand. The relationships presented in Figure 8 have been obtained by accounting for the fact that different portions of the domain can have very different water depths; therefore, the bed level has been divided into depth ranges of around 10cm; each depth interval was then associated to average values for the hydrodynamic variables of interest, and average sediment fractions percentages. Similar relationships can be found without considering depth intervals (Figure S2), indicating that these correlations stand over areas with different features such as water depth, vicinity to the coastline, and sediment sources proximity; however, the latter might be relevant and responsible for data noise.

Residual sediment transport patterns for the spring tidal cycle of interest (11 February 2009) are presented in figure 9. The first set of panels (A to D) refers to the residual suspended load transport, while the second set (E to H) refers to the residual bed load. Residual bed load and suspended load are presented for both spring and neap tide. During neap tide both bed load and suspended load transport patterns are one order of magnitude lower than during spring tide. For each sediment fraction, the highest transport rates are throughout Lowestoft and Dover. Due to the lower settling velocity, the residual suspended transport of mud is higher

and more uniformly distributed around the domain, as compared with other fractions whose residual transport appears patchier.

Figure 10 illustrates morphological changes in the area after one year of simulation and by using a morphological scale factor of 100; the morphological changes might thus be considered representative of the ones occurring over a century. Morphological changes occur at a time scale which is much longer (ranging from months to century), with respect to the time scale of the hydrodynamics. For this reason, morphological acceleration factors are widely used; values of the order of 100 are common for coastal areas simulations, and can be generally used without changing the solution of the problem (Lesser et al., 2004). Changes occurring during one tidal cycle can be assumed to have occurred after 100 tidal cycles in real life, and the number of time steps is thus reduced by a factor of 100 compared to a full 1:1 simulation (Lesser et al., 2004; Latteux, 2005). Noteworthy, morphological changes occur in the northeastern portion of the domain with the deposition of new and accretion of existing offshore sandbanks, which are a typical feature of the area. While sandbanks tend to accrete, there is a slight steepening and erosion of areas located more nearby the coastline. The central part of the domain, which is covered by the higher resolution grid (Figure 10 C, D), is also characterized by a marked steepening of the mouth ridges which become more defined with higher central islands and deeper surrounding channels. New small ridges also start forming around and above 52 degree latitude (panels C, D). Slight changes and a relatively low seaward advancement of areas shallower than 20 m occur in the most south portion of the domain. Qualitative agreement can be found between the coastline erosion predicted by the model and beach profiles collected along the Suffolk coastline since 1991 at around 1km intervals and according to which nearly half of the coastline shows an erosional trend for the period from 1991-2011, with the most significant erosion occurring from south of Benabcre ness to the north of Southwold (Environmental Agency, 2011). Qualitative agreement can be

also found between the morphological changes from the numerical model and data presented by Pye and Blott, 2006 in relation to sandbanks located near the Minsmere Reserve. The volume of the latter increased by 2.3% from 1868 to 1992, with sandbanks maintaining their height but also getting narrower; indeed, in 1940, the Sizewell, and Dunwich banks were a unique bank, which by the 1960 became separated. Similarly, sandbanks features predicted by the model tend to become more pronounced, and to increase their elevation while also gradually separating into more distinct and new features (e.g. Figure 10D). For the offshore sandbanks in the northeaster part of the model domain, results are supported by DTM-derived bathymetric charts for the period from 1846 to 2000 (Horrillo-Caraballo and Reeve, 2008), showing a consistent trend in sandbanks elevation increase and enlargement.

The morphological changes observed in Figure 10 were correlated with the same variables than the sediment fraction availability at the bottom, i.e. intensity of residual currents, mean shear stress, and maximum shear stress during the spring tide (Figure 11). A significant relationship between morphological changes and these variables is found and the highest correlation coefficient (0.96) is found for mean shear stress values and bed elevation changes.

Results from Lanzoni and Seminara, 2002, Toffolon and Lanzoni, 2010, and Seminara et al., 2010 suggest that in tidally dominated systems the morphological evolution of the bottom asymptotically tends toward a dynamic equilibrium configuration characterized by a relatively small and spatially constant residual sediment flux. The hypothesis of dynamic equilibrium conditions has been initially explored for single funnel-shaped channels, and has been later extended to whole systems, such as the Gange Delta, Bangladesh (Fagherazzi, 2008), and Fly river delta, Papua New Guinea (Canestrelli et al., 2010), as well as to conditions were a riverine flow is also present (e.g., Bolla Pittaluga et al., 2015). Figure 12, shows the cumulative frequency distribution of the total residual sediment transport for spring tide, before and after the morphological evolution of the system, e.g. same hydrodynamic

374 forcing, but different bathymetries (Figure 10). It can be noticed that once the system has
375 morphologically evolved, the cumulative distribution becomes narrower (similar residual
376 transport everywhere), and skewed toward smaller values, which is in agreement with
377 literature results for other environments suggesting the tendency of the system to approach a
378 dynamic equilibrium configurations.

379

380 **Discussion**

381 In this paper we have been focusing on the coastline of SE England, and investigated residual
382 transport patterns, their connection to the availability of sediments within the domain, as well
383 as the morphological evolution of the area.
384 Results in relation to the morphological evolution of the system and sediment transport
385 patterns suggest that, under tidally dominated conditions, the system might tend toward a
386 dynamic equilibrium configuration characterized by relatively small and spatially constant
387 residual sediment fluxes (e.g. Lanzoni and Seminara, 2002; Toffolon and Lanzoni, 2010).
388 Indeed, numerical results suggest that when the same hydrodynamic forcing is applied to the
389 system after a long term, century scale, morphological evolution, the residual transport of
390 sediments is more uniformly distributed and smaller (Figure 12). Previous work on tidal
391 channels has shown that this equilibrium condition is controlled by the temporal symmetry of
392 the flow field as suggested by the numerical solution of the one-dimensional equations, as
393 well as by field observations (Lanzoni and Seminara, 2002; Seminara et al., 2010). It has
394 been also noted that this dynamic equilibrium condition is compatible with the higher order
395 contributions of settling and scour effects to the channel profile (Pritchard and Hogg, 2003).
396 It is also worthwhile to observe that a real equilibrium condition is only asymptotically
397 achieved and, for real scenarios, an evolution of the system is generally present due to
398 variations into external forcing induced, for instance, by storms occurrence or relative sea

level variations (e.g. Pritchard and Hogg, 2003; Toffolon and Lanzoni, 2010; Canestrelli et al., 2010).

Among the others, uncertainties in relation to riverine inputs and surge occurrence are important to evaluate when making considerations in regard to the achievement of an equilibrium configuration.

We found that residual currents magnitude maintains a similar spatial distribution during spring and neap tide, with maximum values occurring around Lowestoft and north of Dover. Average residual currents intensities increase up to 113% during the spring tide. The highest differences in residual currents occur in the deepest portions of the domain, and a significant relationship exists between differences in the intensity of residuals during neap and spring tides, and water depth. Changes in the direction of residual currents also occur when transitioning from neap to spring tide: during the neap tide, the majority of residuals are directed northeastwards, while during the spring tide a bimodal distribution in residual currents direction is present, with many locations characterized by southerly oriented residuals, and large portions of the Thames estuary becoming flood-dominated, especially the channels areas.

Flood/ebb dominance and the direction of residual currents in general are relevant for the net transport of sediments. Results presented in this manuscript demonstrate that residual currents can significantly change from neap to spring tide. We suggest that these differences should be taken into account when considering the interaction of the tidal flow with nonperiodic, and irregular sediment signals such as riverine inputs, or sediment resuspension by storms in order to understand whether these can effectively function as sediment sources to the shoreline.

The intensity of residuals was found to be an indicator of sediment fractions availability at the bottom. Specifically, a significant negative correlation was found between the intensity of

424 residual currents and the percentage of mud, and a positive correlation was found between the
425 percentage of available gravel and sand and the residuals. Understanding the spatial
426 distribution of sediment grain size is relevant to determine locations where sediments can be
427 more easily re-suspended and to possibly determine the spatial distribution of pollutants
428 which are more likely to adhere to mud due to its cohesiveness and chemical properties (e.g.
429 Wolanski et al., 2000). Residual currents can be thus considered as a possible indicator to
430 localize the deposition of the finest fractions, and possible pollutants accumulations.
431 For the Thames region residual currents are characterized by the formation of clockwise
432 eddies in agreement with existing literature data and theoretical studies according to which
433 residual eddies can form due to the interaction of the oscillating flow with a varying
434 bathymetry, and are caused by the imbalance between out-flux and influx vorticity trough the
435 ridge contour (e.g. Zimmerman, 1981; Dyer and Huntley, 1997; Horillo-Caraballo and Revee,
436 2008). Residual sediment transport patterns and morphological changes for the area have
437 been also simulated by taking into account the presence of the different sediment fractions at
438 the bottom. In terms of morphological changes, a numerical simulation intended to account
439 for morphological changes over a century timescale was conducted. Numerical models like
440 the one presented in this paper, can be useful tools to investigate complex hydrodynamic and
441 sediment transport dynamics, but results always need to be treated cautiously.
442 Particularly in terms of sediment dynamics, large uncertainties exist in regard to the complex
443 sediment budget in the area, that might have not been fully reproduced within the present
444 modelling framework. Uncertainties also come from the fact that some sediment fluxes
445 including sources from rivers, seabed erosion, and cliff erosion might be difficult to quantify.
446 For instance, the resolution of the domain, as well as the modelled dynamics, might have
447 underestimated the amount of fluxes coming from the erosion of soft cliffs. Furthermore,
448 residual currents are second order features, and some inaccuracy in their representation might

449 come from even very small errors into the velocity field. Another limitation comes from the
450 fact that this modelling framework only accounts for water level changes and does not
451 consider wind generated waves, and the littoral drift. Considering the vertical structure
452 associated to waves velocity, the latter are expected to be mainly relevant for the shallower
453 areas, while their contribution to well submerged banks might be secondary with respect to
454 tidal motion (Horillo-Caraballo and Reeve, 2008).
455 Wind waves can increase bottom shear stress, enhance both sediments resuspension and
456 erosion, and contribute to the littoral drift; in this sense waves can be responsible for changes
457 in sediment pathways, as well as sediment recirculation within sand bank systems (e.g. Lee et
458 al., 2004). For example, Christie et al., 1999 used short term measurements to show that for
459 the Humber Estuary (UK), typical tidal currents were causing accretions of the order of few
460 millimetres and onshore fluxes, while waves can cause the erosion of several centimetres of
461 sediments and an increase in seaward transport. However, the effects of short term wave
462 events tended to cancel out in time such that net seasonal changes were of the order of calm
463 conditions (Christie et al., 1999). Waves can be also important when dealing with the
464 sandbanks-shoreline interaction, as debate is present on whether the presence of sandbanks
465 could reduce wave action and, as a consequence, shoreline erosion (e.g. Pye and Blott.,
466 2006). For instance, Robinson et al., 1980, sustained that a reduction in coastline erosion was
467 attributable to the growth of sandbanks, and their reduction in wave energy, while Halcrow
468 Maritime, 2000 concluded that the sandbanks are not as important in reducing the energy that
469 reaches the shoreline under normal weather conditions.
470 In terms of riverine inputs, for the Thame estuary, which occupy large part of the modelled
471 domain, the flow rate is relatively small and generally vary between a 10 percentile of $10 m^3/s$
472 to a 95 percentile of 0.97 m^3/s, with a mean of 3.9 m^3/s (e.g. Neal et al., 2005). For the
473 coastline as a whole, the fluvial sediment supply is generally considered negligible (e.g.

McCave, 1987). Nevertheless, riverine inputs, especially during large floods can affect both the hydrodynamic and morphodynamic features of a system. From a morphodynamic point of view, under macro tidal conditions, the presence of a riverine flow has been found to promote shoal widening and an initial faster accretion of sand deposits, producing wider and shallower shoals (Leonardi et al., 2013). Horrevoets et al., 2004 demonstrated analytically that river discharge influences tidal damping, and that the critical point starting from which the system becomes river dominated depends on flow magnitude, with the effect of riverine flow being friction dominated. Using ADCP field measurements it has been shown that even in micro-tidal and very shallow conditions, residual currents can be relevant and that under extreme river discharge periods, residual currents are amplified and almost double with respect to the no-discharge case, and this can contributed to an outward transport of sediments (Leonardi et al., 2015).

Morphological results indicate a steepening of existing sand banks, especially in the Thames and in the northeastern portion of the domain, where the existing banks tend to become higher and more pronounced and new ones tend to form. For the northeastern portion of the study area, the coastlines adjacent to the accreting sand banks tend to partially erode, while no significant sediment removal from the coastline areas can be noticed for the southernmost portion. The enhancement of sandbanks features has been connected to residual currents exhibiting closed circulation patterns having direction parallel to the shore; in fact, the convergence of the circulating stream causes the potential accumulation of sand on the top of sand banks. The existence of circulation gyres has been long recognized (e.g. Zimmermann, 1981); for this test case, the major axis of the main recirculating gyres ranged from around 10 to 35 km, and the minor axis ranged from around 2 to 4 km. This is relevant considering the economic importance of sand banks which are a cause of refraction for incoming waves and

498 can help protecting many shoreline stretches form erosion; on the other hand, banks might
499 also create hazards to navigation.
500
501 **Conclusions**
502 The coastline of SE England was used as a test case to investigate possible changes in
503 residual currents, and residual transport patterns from neap to spring tide, the reciprocal
504 interaction between residuals and the character of the bed, and the morphological evolution of
505 the coastline at a century timescale. The numerical model Delft 3D was used for this
506 investigation.
507 We found that the intensity of residual currents maintains a similar spatial distribution
508 during both spring and neap tide, with maximum values occurring around Lowestoft and
509 north of Dover. The average intensity of residual currents is doubled during spring tide. The
510 highest differences in residuals occur in the deepest portions of the domain, and a significant
511 relationship exists between differences in the intensity of residual currents during neap and
512 spring tides, and water depth.
513 The intensity of residuals was found to be an indicator of sediment fractions
514 availability at the bottom. Specifically, a significant negative correlation was found between
515 the intensity of residual currents and the percentage of mud, and a positive correlation was
516 found between the percentage of available gravel and sand and the residuals.
517 Changes in the direction of residual currents also occur when transitioning from neap
518 to spring tide; for instance, during spring tide, large portions of the Thames estuary become
519 flood-dominated, especially the channels areas.
520 For the Thames region residual currents are also characterized by the formation of
521 clockwise eddies in agreement with existing literature data and theoretical studies according
522 to which residual eddies can form due to the interaction of the oscillating flow with a varying

bathymetry, and are caused by the imbalance between out-flux and influx vorticity trough the ridge contour.

In terms of morphological changes, a numerical simulation intended to account for morphological changes over a century timescale was conducted, suggesting that the morphological evolution of the system tends to enhance sand banks features, with an increase in elevation and steepening of the bank contours. Furthermore, the long term the morphology of the system evolves toward a dynamic equilibrium configuration characterized by smaller, and spatially constant residual transport patterns.

Acknowledgment

All data are available upon request to the first Author. This work was partially supported by the NERC Award: NE/N015614/1. We acknowledge the MET office for providing pressure and wind data for this model, the British Geological Survey (BGS) for the GIS-maps for the bed, and the UK Hydrographic Office for the VORF corrections.

References

Androsov, A.A., Kagan, B.A., Romanenkov, D.A. and Voltzinger, N.E., 2002. Numerical modelling of barotropic tidal dynamics in the strait of Messina. Advances in water resources, 25(4), pp.401-415.

Allen, J.I., Somerfield, P.J. and Gilbert, F.J., 2007. Quantifying uncertainty in high-resolution coupled hydrodynamic-ecosystem models. Journal of Marine Systems, 64(1), pp.3-14.

Bolla Pittaluga, M., Tambroni, N., Canestrelli, A., Slingerland, R., Lanzoni, S. and Seminara, G., 2015. Where river and tide meet: The morphodynamic equilibrium of alluvial estuaries. Journal of Geophysical Research: Earth Surface, 120(1), pp.75-94.

Brooks, S.M., Spencer, T. and Christie, E.K., 2017. Storm impacts and shoreline recovery: Mechanisms and controls in the southern North Sea. Geomorphology, 283, pp.48-60.

Brooks, S.M. and Spencer, T., 2014. Importance of decadal scale variability in shoreline response: examples from soft rock cliffs, East Anglian coast, UK. Journal of coastal conservation, 18(5), pp.581-593.

552 Canestrelli, A., Fagherazzi, S., Defina, A. and Lanzoni, S., 2010. Tidal hydrodynamics and
553 erosional power in the Fly River delta, Papua New Guinea. Journal of Geophysical
554 Research: Earth Surface, 115(F4).
555 Canestrelli, A., Lanzoni, S. and Fagherazzi, S., 2014. One-dimensional numerical modeling
556 of the long-term morphodynamic evolution of a tidally-dominated estuary: The Lower
557 Fly River (Papua New Guinea). Sedimentary Geology, 301, pp.107-119.
558 Chan, T.F. and Mathew, T.P., 1994. Domain decomposition algorithms. Acta numerica, 3,
559 pp.61-143.Christie, M.C., Dyer, K.R. and Turner, P., 1999. Sediment flux and bed level
560 measurements from a macro tidal mudflat. Estuarine, Coastal and Shelf Science, 49(5),
561 pp.667-688.
562 Dyer, K.R. and Huntley, D.A., 1999. The origin, classification and modelling of sand banks
563 and ridges. Continental Shelf Research, 19(10), pp.1285-1330.
564 Dyer, K.R. and Moffat, T.J., 1998. Fluxes of suspended matter in the East Anglian plume
565 Southern North Sea. Continental Shelf Research, 18(11), pp.1311-1331.
566 Defne, Z. and Ganju, N.K., 2015. Quantifying the residence time and flushing characteristics
567 of a shallow, back-barrier estuary: application of hydrodynamic and particle tracking
568 models. Estuaries and Coasts, 38(5), pp.1719-1734.
569 Environmnetal agency, 2011. Coastal Trends Report. Suffolk RP022/S/2011.
570 Hackney, C., Darby, S.E. and Leyland, J., 2015. Landscapes on the edge: examining the role
571 of climatic interactions in shaping coastal watersheds using a coastal–terrestrial
572 landscape evolution model. Earth Surface Processes and Landforms, 40(3), pp.313-325.
573 Halcrow Maritime, 2000. Lowestoft to Thorpeness Coastal Process/Strategy Study. Part 2.
574 Swindon, UK: Strategy Assessment, Report.
575 Hydraulics, D., 2014. Delft3D-FLOW User Manual: Simulation of multi-dimensional
576 hydrodynamic flows and transport phenomena. including sediments. Technical report.
577 Horrillo-Caraballo, J.M. and Reeve, D.E., 2008. Morphodynamic behaviour of a nearshore
578 sandbank system: The Great Yarmouth Sandbanks, UK. Marine Geology, 254(1), pp.91-
579 106.
580 Jude, S., Jones, A.P., Andrews, J.E. and Bateman, I.J., 2006. Visualisation for participatory
581 coastal zone management: a case study of the Norfolk Coast, England. Journal of coastal
582 research, pp.1527-1538.
583 Krone, R.B., 1962. Flume studies of the transport of sediment in estuarial shoaling processes.
584 Lanzoni, S. and Seminara, G., 2002. Long-term evolution and morphodynamic equilibrium of
585 tidal channels. Journal of Geophysical Research: Oceans, 107(C1).

586 Latteux, B., 1995. Techniques for long-term morphological simulation under tidal action.
587 Marine Geology, 126(1-4), pp.129-141.
588 Lee, H.J., Jo, H.R., Chu, Y.S. and Bahk, K.S., 2004. Sediment transport on macrotidal flats in
589 Garolim Bay, west coast of Korea: significance of wind waves and asymmetry of tidal
590 currents. Continental Shelf Research, 24(7), pp.821-832.
591 Lesser, G.R., Roelvink, J.A., Van Kester, J.A.T.M. and Stelling, G.S., 2004. Development
592 and validation of a three-dimensional morphological model. Coastal engineering, 51(8),
593 pp.883-915.
594 Leonardi, N., Canestrelli, A., Sun, T. and Fagherazzi, S., 2013. Effect of tides on mouth bar
595 morphology and hydrodynamics. Journal of Geophysical Research: Oceans, 118(9),
596 pp.4169-4183.
597 Leonardi, N., Kolker, A.S. and Fagherazzi, S., 2015. Interplay between river discharge and
598 tides in a delta distributary. Advances in Water Resources, 80, pp.69-78.
599 Liang, D., Wang, X., Bockelmann-Evans, B.N. and Falconer, R.A., 2013. Study on nutrient
600 distribution and interaction with sediments in a macro-tidal estuary. Advances in water
601 resources, 52, pp.207-220.
602 Mathis, M., Elizalde, A., Mikolajewicz, U. and Pohlmann, T., 2015. Variability patterns of
603 the general circulation and sea water temperature in the North Sea. Progress in
604 Oceanography, 135, pp.91-112.
605 McCave, I.N., 1987. Fine sediment sources and sinks around the East Anglian Coast (UK).
606 Journal of the Geological Society, 144(1), pp.149-152.
607 Murphy, A.H., and E.S. Epstein. 1989. Skill scores and correlation coefficients in model
608 verification. Monthly Weather Review 117:572–581.
609 Neal, C., Neal, M., Hill, L. and Wickham, H., 2006. The water quality of the River Thame in
610 the Thames Basin of south/south-eastern England. Science of the Total Environment,
611 360(1), pp.254-271.
612 Parker, B.B., 1991. Tidal interactions. Tidal hydrodynamics, 237.
613 Partheniades, E., 1965. Erosion and deposition of cohesive soils. Journal of the Hydraulics
614 Division, 91(1), pp.105-139.
615 Pawlowicz, R., Beardsley, B. and Lentz, S., 2002. Classical tidal harmonic analysis including
616 error estimates in MATLAB using T_TIDE. Computers & Geosciences, 28(8), pp.929-
617 937.
618 Partheniades, E., 1965. Erosion and deposition of cohesive soils. Journal of the Hydraulics
619 Division, 91(1), pp.105-139.

620 Pawlowicz, R., Beardsley, B. and Lentz, S., 2002. Classical tidal harmonic analysis including
621 error estimates in MATLAB using T_TIDE. Computers & Geosciences, 28(8), pp.929-
622 937.
623 Pingree, R.D. and Maddock, L., 1985. Rotary currents and residual circulation around banks
624 and islands. Deep Sea Research Part A. Oceanographic Research Papers, 32(8), pp.929-
625 947.
626 Pye, K. and Blott, S.J., 2006. Coastal processes and morphological change in the Dunwich-
627 Sizewell area, Suffolk, UK. Journal of Coastal Research, pp.453-473.
628 Pritchard, D. and Hogg, A.J., 2003. Cross-shore sediment transport and the equilibrium
629 morphology of mudflats under tidal currents. Journal of Geophysical Research:
630 Oceans, 108(C10).
631 Ralston, D.K.,W.R. Geyer, and J.A. Lerczak. 2010. Structure, variability, and salt flux in a
632 strongly forced salt wedge estuary. Journal of Geophysical Research 115, C06005.
633 doi:10.1029/2009JC005806.
634 Robinson, A.H.W., 1966. Residual currents in relation to shoreline evolution of the East
635 Anglian coast. Marine Geology, 4(1), pp.5767-6384.
636 Roelvink, J.A., 2006. Coastal morphodynamic evolution techniques. Coastal Engineering,
637 53(2), pp.277-287.
638 Van Rijn, L.C., 1984. Sediment transport, part I: bed load transport. Journal of hydraulic
639 engineering, 110(10), pp.1431-1456.
640 Van Rijn, L.C., 1993. Principles of sediment transport in rivers, estuaries and coastal seas
641 (Vol. 1006). Amsterdam: Aqua publications.
642 Rijn, L. C. van, D. R. Walstra and M. v. Ormondt, 2004. Description of TRANSPOR2004
643 and implementation in Delft3D-ONLINE. Tech. Rep. Z3748.10, WL | Delft
644 Hydraulics, Delft, The Netherlands. 69, 85, 237, 239.
645 Van Rijn, L.C., Walstra, D.J.R., Grasmeijer, B., Sutherland, J., Pan, S. and Sierra, J.P., 2003.
646 The predictability of cross-shore bed evolution of sandy beaches at the time scale of
647 storms and seasons using process-based profile models. Coastal Engineering, 47(3),
648 pp.295-327.
649 Robinson, A.H.W., 1980. Erosion and accretion along part of the Suffolk coast of East
650 Anglia, England. Marine Geology, 37(1-2), pp.133-146.
651 Robinson, C., Li, L. and Barry, D.A., 2007. Effect of tidal forcing on a subterranean estuary.
652 Advances in Water Resources, 30(4), pp.851-865.

Roelvink, J.A., 2006. Coastal morphodynamic evolution techniques. Coastal Engineering, 53(2), pp.277-287.

Roos, P.C., Velema, J.J., Hulscher, S.J. and Stolk, A., 2011. An idealized model of tidal dynamics in the North Sea: resonance properties and response to large-scale changes. Ocean dynamics, 61(12), pp.2019-2035.

Sanford, L.P. and Halka, J.P., 1993. Assessing the paradigm of mutually exclusive erosion and deposition of mud, with examples from upper Chesapeake Bay. Marine Geology, 114(1-2), pp.37-57.

Schans, H., Möller, I. and Spencer, T., 2001. Large-scale classification of the East Anglian coastline, UK. In Coastal Dynamics' 01 (pp. 683-692).

Seminara, G., Lanzoni, S., Tambroni, N. and Toffolon, M., 2010. How long are tidal channels?. Journal of Fluid Mechanics, 643, pp.479-494.

Stanev, E.V., Dobrynin, M., Pleskachevsky, A., Grayek, S. and Günther, H., 2009. Bed shear stress in the southern North Sea as an important driver for suspended sediment dynamics. Ocean Dynamics, 59(2), pp.183-194.

Svendsen, E. and Mork, M., 1991. Features of the northern North Sea circulation. Continental Shelf Research, 11(5), pp.493-508.

Sutherland, J., A.H. Peet, and R.L. Soulsby. 2004. Evaluating the performance of morphological models. Coastal Engineering 51(8–9): 917–939.

Toffolon, M. and Lanzoni, S., 2010. Morphological equilibrium of short channels dissecting the tidal flats of coastal lagoons. Journal of Geophysical Research: Earth Surface, 115(F4).

Williams, J.J., MacDonald, N.J., O'Connor, B.A. and Pan, S., 2000. Offshore sand bank dynamics. Journal of Marine Systems, 24(1), pp.153-173.

Winther, N.G. and Johannessen, J.A., 2006. North Sea circulation: Atlantic inflow and its destination. Journal of Geophysical Research: Oceans, 111(C12).

Winterwerp, J.C., 2007. On the sedimentation rate of cohesive sediment, Proceedings in Marine Science, 8, pp. 209-226.

Wolanski, E. and Spagnol, S., 2000. Pollution by mud of Great Barrier Reef coastal waters. Journal of Coastal Research, pp.1151-1156.

Zimmerman, J.T.F., 1981. Dynamics, diffusion and geomorphological significance of tidal residual eddies. Nature, 290(5807), pp.549-555.

687 **Figure captions**

688 Figure 1 A) Location of the study area (red box); solid lines are co-phase lines, and dashed
689 lines are co-range lines (values in cm) (adapted from Roos et al., 2011). B, C) Model domain;
690 red, and blue contours indicate model exterior, and interior boundaries respectively. Blue
691 points indicate buoy stations: Cromer (CRO), Lowestoft (LOW), Dover (DOV), Newhaven
692 (NEW), Sheerness (SHEER) C) Higher resolution domain: the area within blue lines is the
693 one indicated in panel B.

694

695 Figure 2 Percentage values of the sediment fractions at the bottom.

696

697 Figure 3 Modelled water levels (red line), and Buoys data (blue points). Station locations is
698 indicated in Figure 1B.

699

700 Figure 4 Maximum bed shear stress values during neap (A, D) and spring tide (B, E), and
701 their difference (C, F). The second row of panels refers to the higher resolution domain.

702

703 Figure 5 Residual currents during neap tide (A, D, E), spring tide (B, F, G), and their
704 difference (C). The second row of panels refers to the higher resolution domain. Background
705 colours refer to the intensity of the residual currents apart from panels E, and G where
706 colours refer to bathymetric values.

707

708 Figure 6 Residual currents direction (panels A, B, E, F), and corresponding frequency
709 magnitude distribution (panels C, D, G and H) .

710

711 Figure 7 Relationship between Bed level (m), and changes in residual currents from neap to
712 spring tide. Grey points refer to the largest domain, while blue points are for the higher
713 resolution domain.
714
715 Figure 8 Relationship between sediment fractions (mud, sand, gravel) availability at the
716 bottom, and the following variables: residual currents intensity (panels A, B, C), mean
717 (panels D, E, F) and maximum bed shear stress (panels G, H, I). Pearson coefficients are
718 always<0.05.
719
720 Figure 9 Residual suspended (panels A, B, C and D) and bed load (panels E, F, G, H)
721 transport ($m^3/s/m$) for different sediment fractions.
722
723 Figure 10 Initial bed level (A), and bed level after one year simulation with 100
724 morphological factor.
725
726 Figure 11 Relationship between morphological changes, and the following: residual currents
727 intensity, mean shear stress and maximum shear stress during spring tide.
728
729 Figure 12 Cumulative distribution of the percentage areas characterized by a given residual
730 total transport before and after the morphological evolution given the same hydrodynamic
731 forcing of the spring tidal cycles considered in the manuscript.
732
733 Table S1 harmonic analysis of Delft3D outputs and buoy data for the five locations indicated
734 in Figure 1b, and the three major harmonic constituents.

735 Figure S1 Difference in modelled water levels, and buoy data (station locations indicated in Figure 1).

Figure S2 Relationship between sediment fractions (mud, sand, gravel) availability at the bottom, and the following variables: residual currents intensity (panels A, B, C), mean (panels D, E, F) and maximum bed shear stress (panels G, H, I). For each panel, first R^2 values refer to the raw data, while values in parenthesis refer to the binned data. Bins have been done by dividing the horizontal axis into 100 regular intervals, and percentage fractions and velocity/ bed shear stress values have been averaged for each bin. Pearson coefficients are always<0.05.

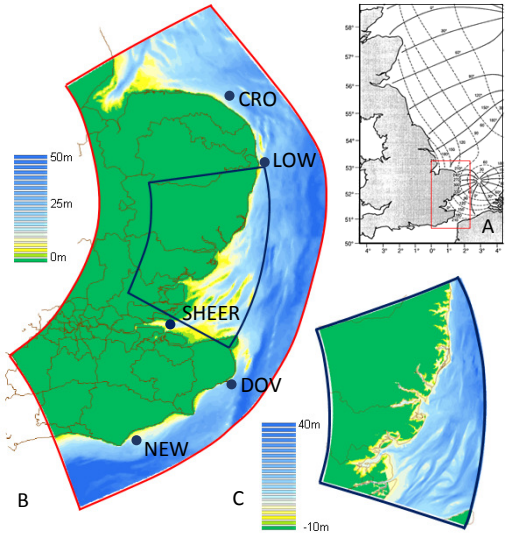
CRO
LOW
SHEER
DOV
NEW
50m
25m
0m
A
B
C
40m
-10m

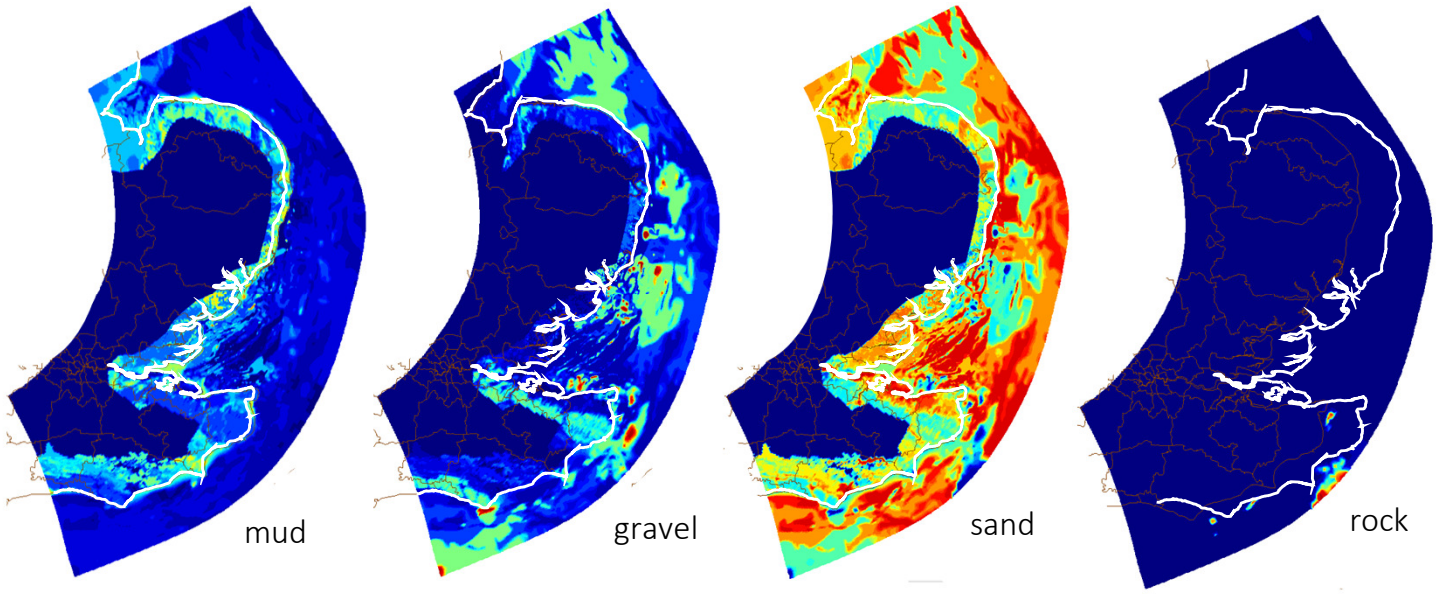
mud
gravel
sand
rock
1
0.5
0

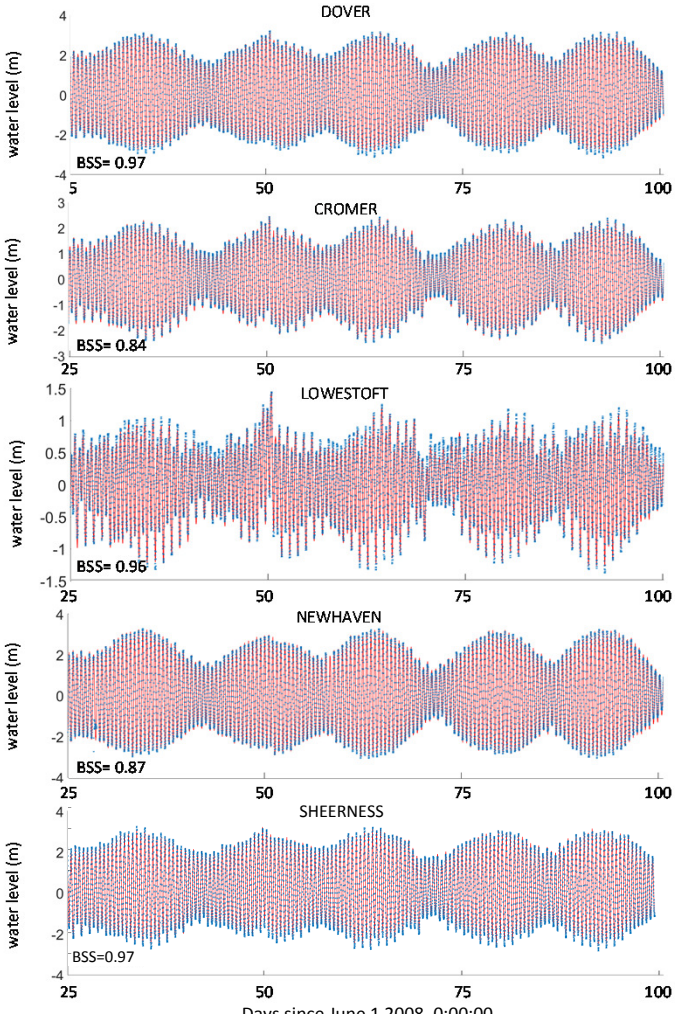
DOVER
water level (m)
BSS= 0.97
CROMER
water level (m)
BSS= 0.84
LOWESTOFT
water level (m)
BSS= 0.96
NEWHAVEN
water level (m)
BSS= 0.87
SHEERNESS
water level (m)
BSS=0.97
Days since June 1 2008, 0:00:00

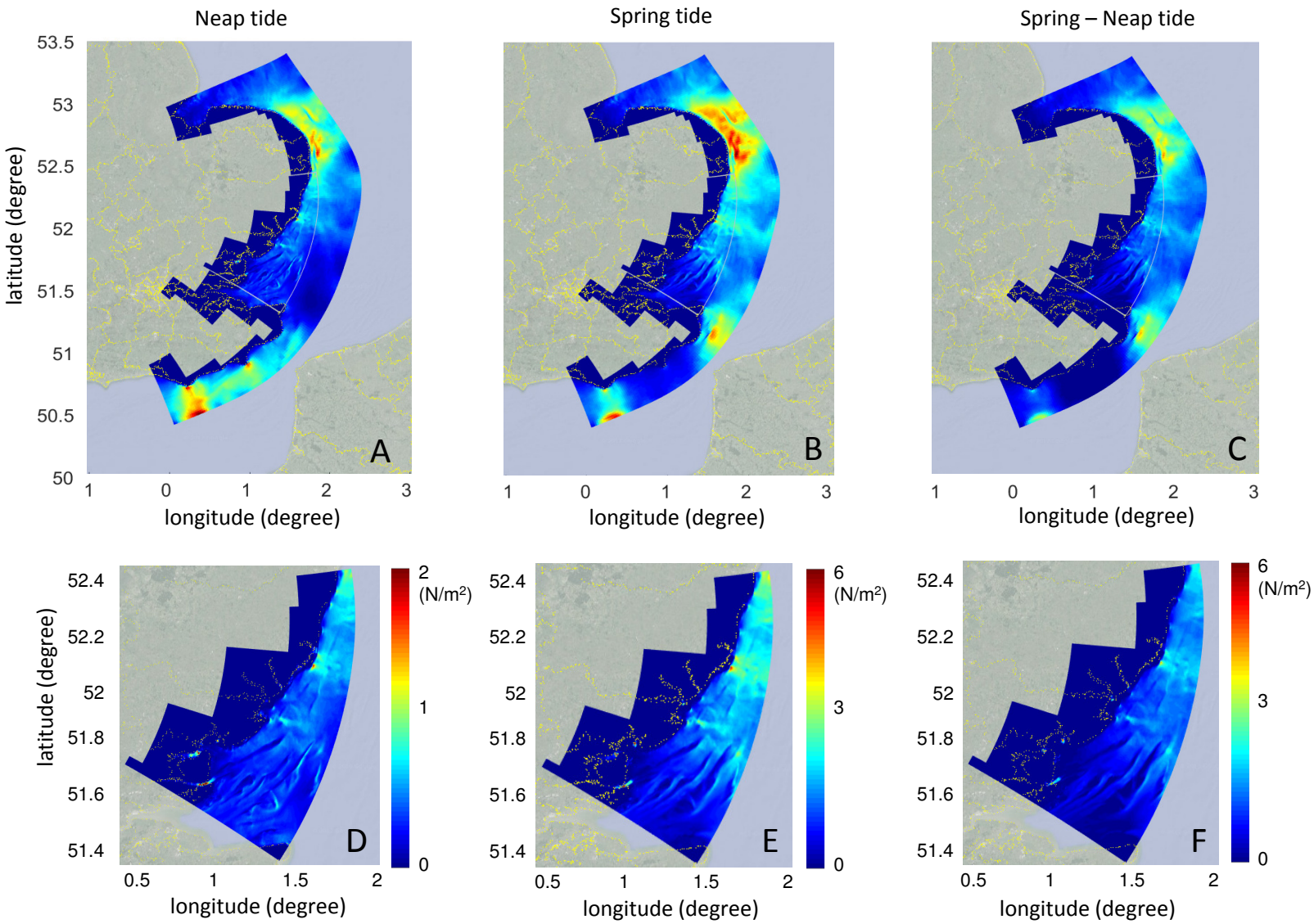
Neap tide
Spring tide
Spring – Neap tide
latitude (degree)
longitude (degree)
A
B
C
D
E
F
(N/m²)

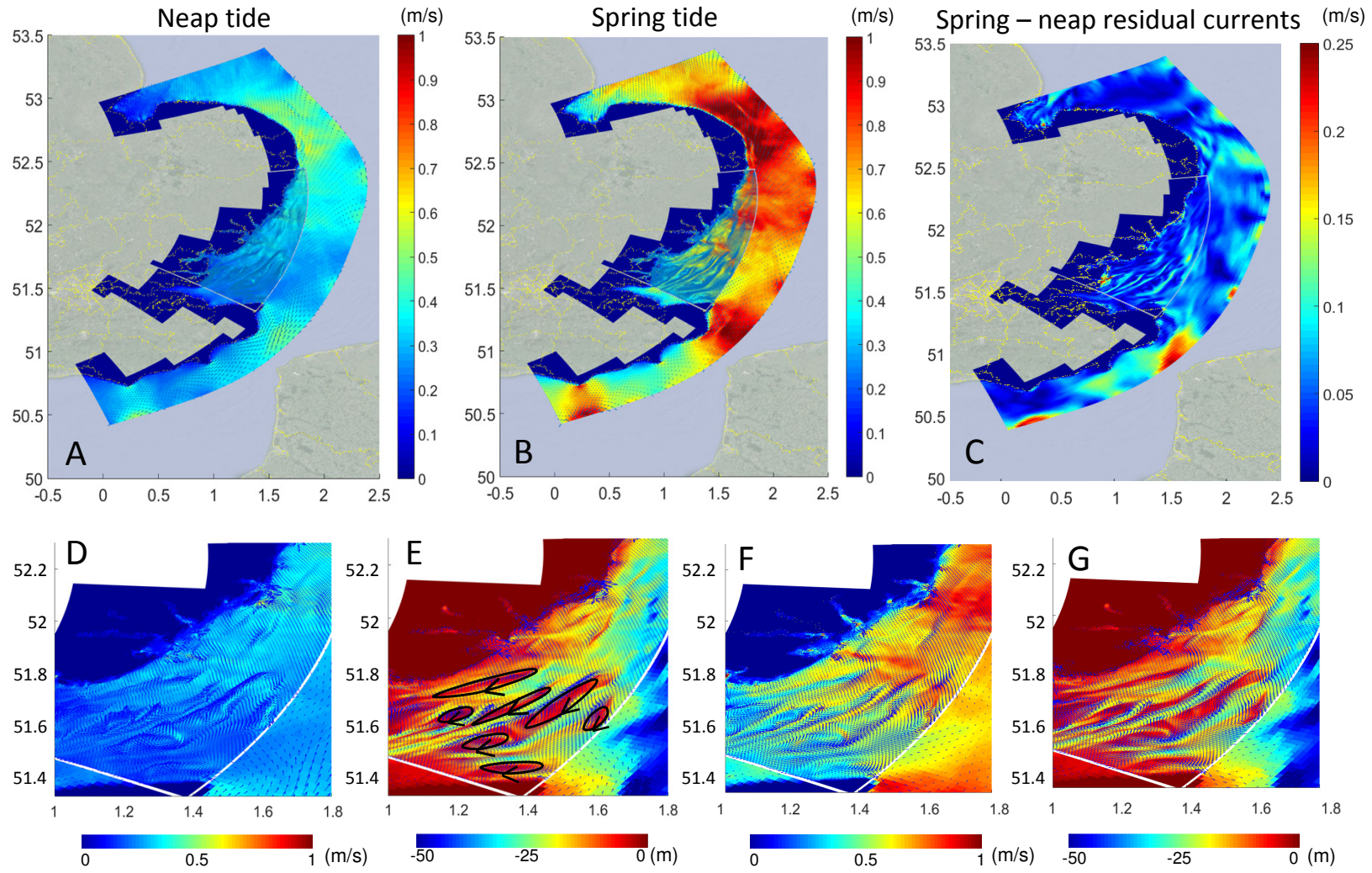
Neap tide
Spring tide
Spring – neap residual currents
(m/s)
A
B
C
D
E
F
G
(m)

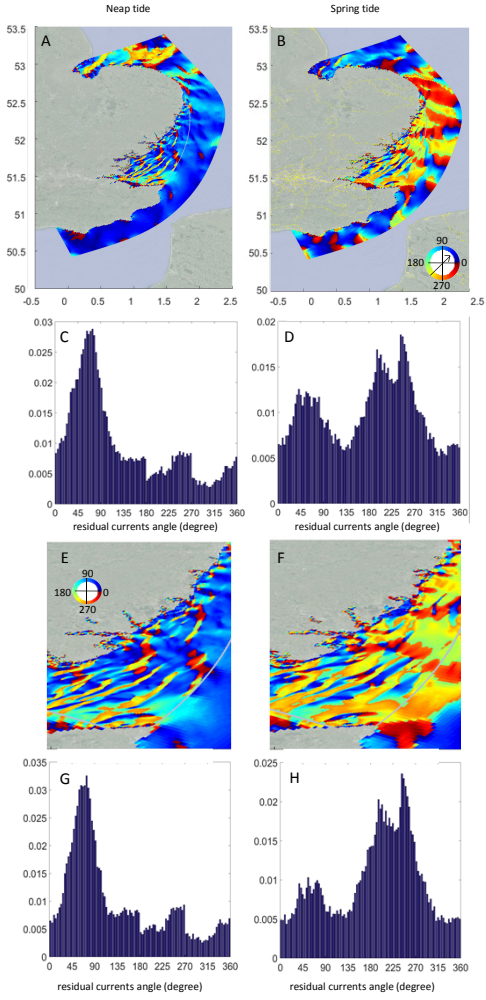
Neap tide
Spring tide
A
B
C
D
E
F
G
H
90
180
0
270
residual currents angle (degree)
residual currents angle (degree)
residual currents angle (degree)
residual currents angle (degree)

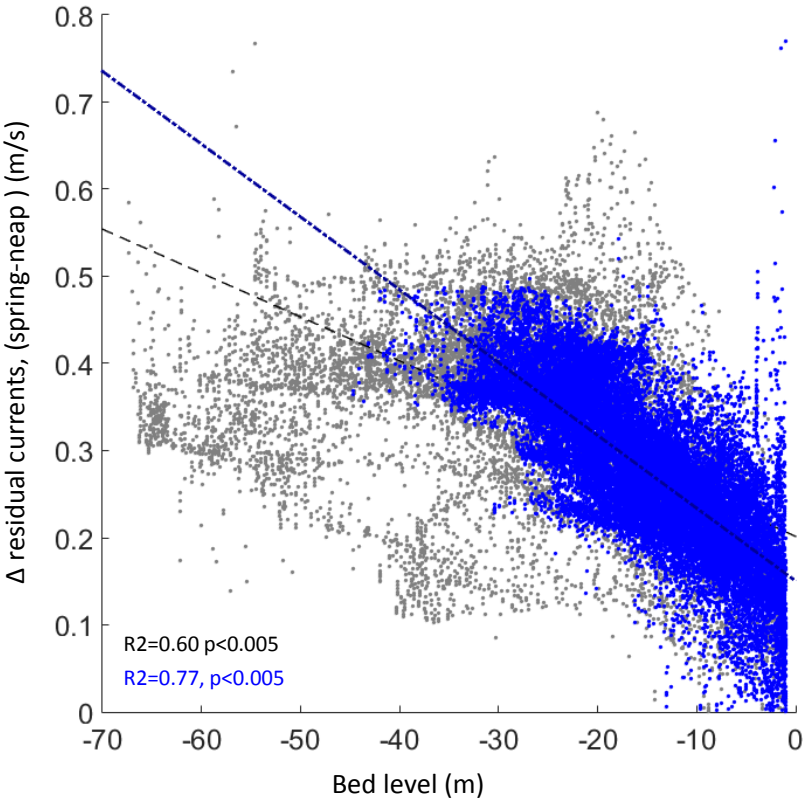
0.8
0.7
0.6
0.5
0.4
0.3
0.2
0.1
0
-70
-60
-50
-40
-30
-20
-10
0
Δ residual currents, (spring-neap) (m/s)
Bed level (m)
R2=0.60 p<0.005
R2=0.77, p<0.005

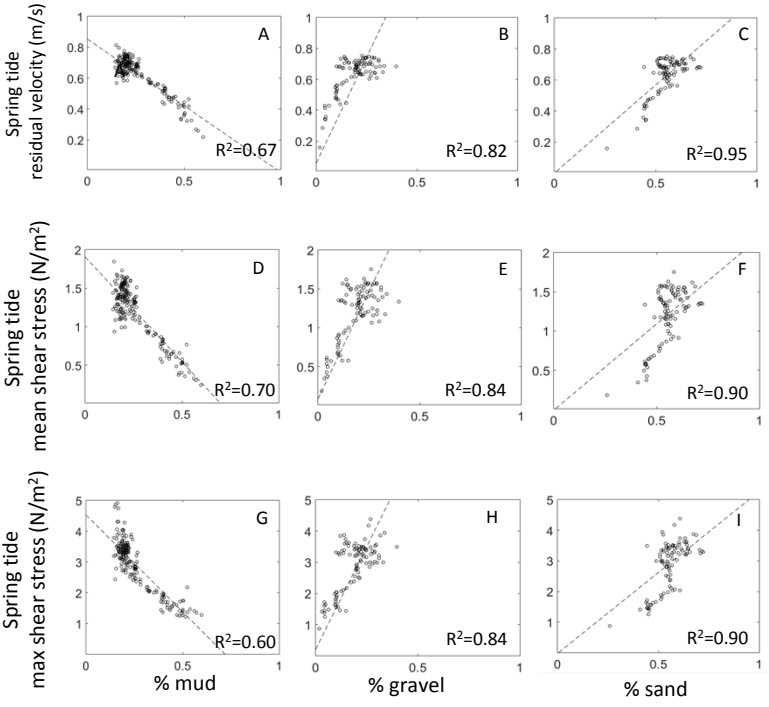
Spring tide
residual velocity (m/s)
A
R²=0.67
B
R²=0.82
C
R²=0.95
Spring tide
mean shear stress (N/m²)
D
R²=0.70
E
R²=0.84
F
R²=0.90
Spring tide
max shear stress (N/m²)
G
R²=0.60
H
R²=0.84
I
R²=0.90
% mud
% gravel
% sand

residual suspended-sediment transport

residual bed load transport

spring tide

neap tide

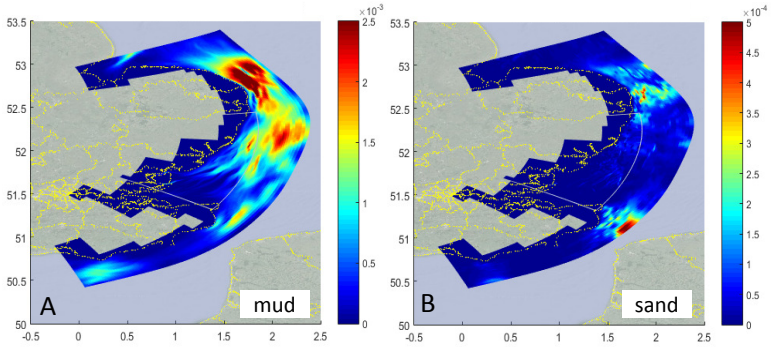

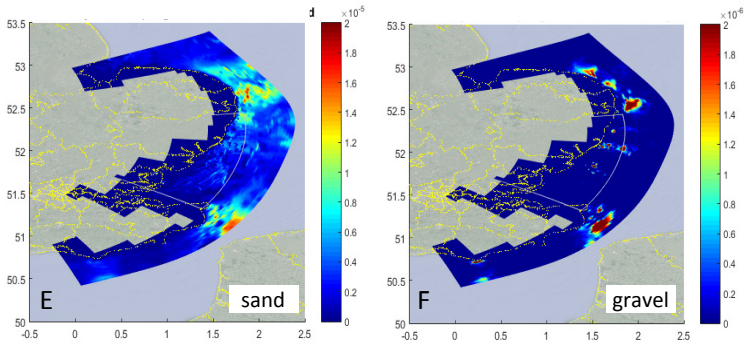

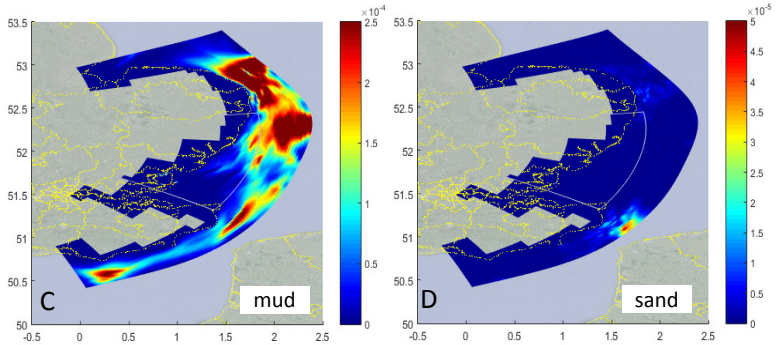

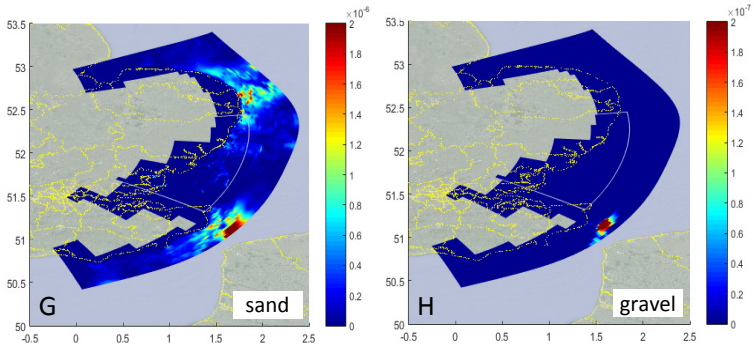

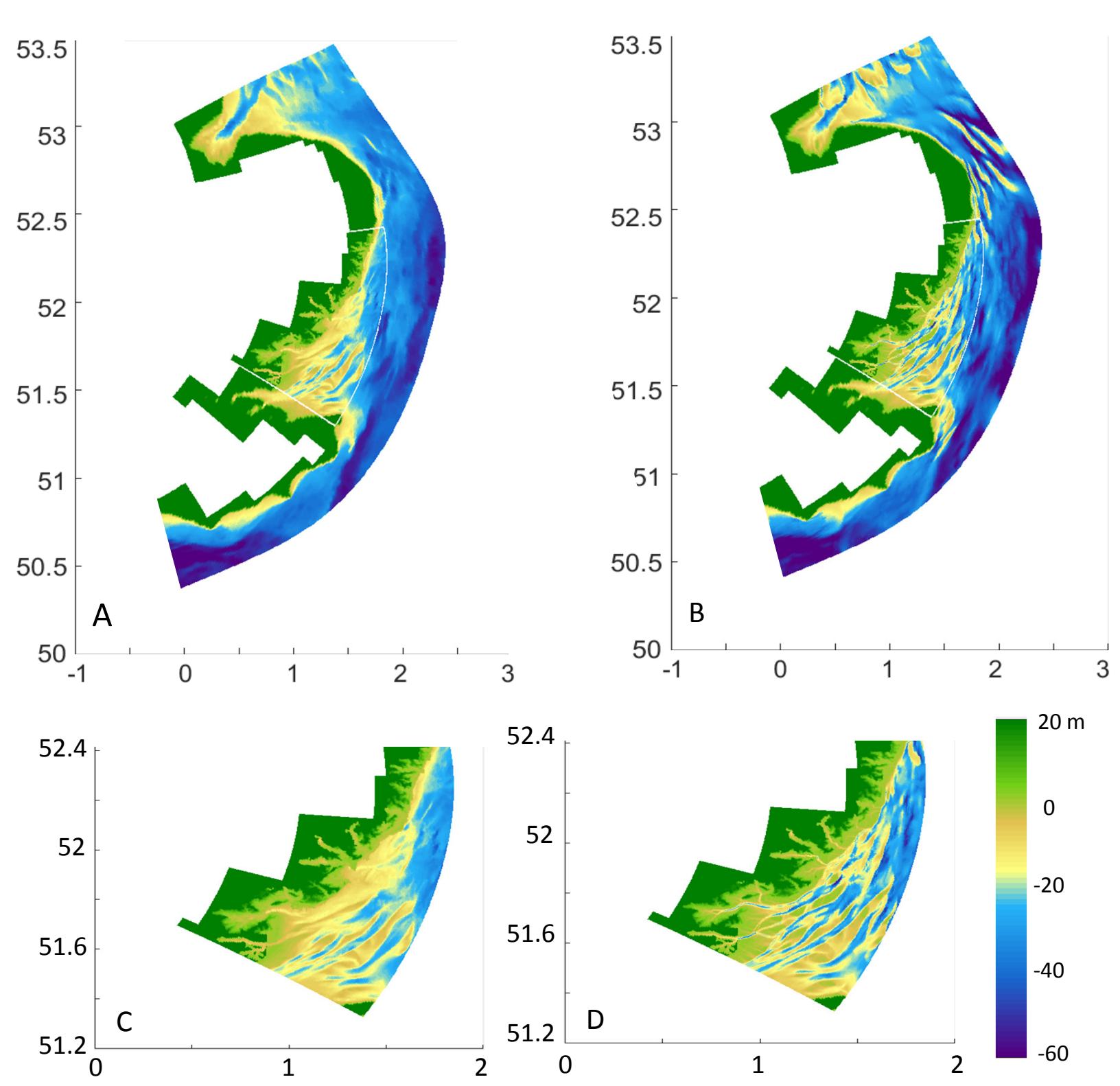
A
B
C
D
20 m
0
-20
-40
-60

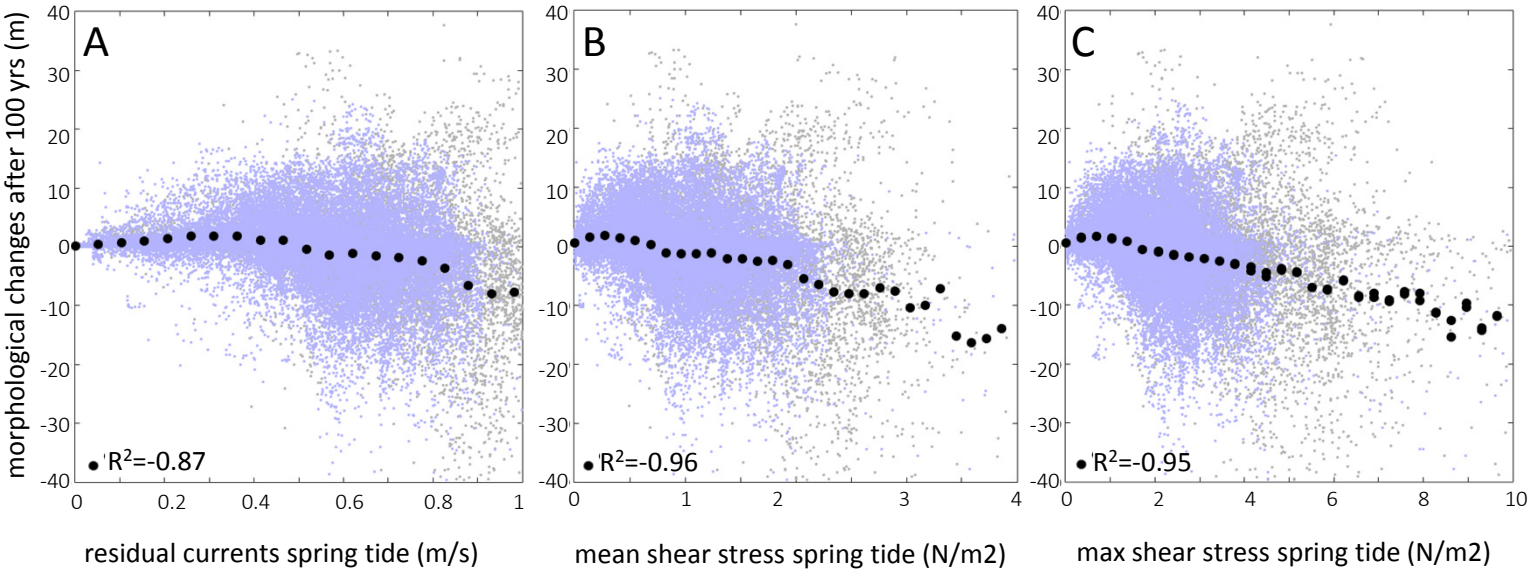
A
B
C
morphological changes after 100 yrs (m)
R²=-0.87
R²=-0.96
R²=-0.95
residual currents spring tide (m/s)
mean shear stress spring tide (N/m2)
max shear stress spring tide (N/m2)

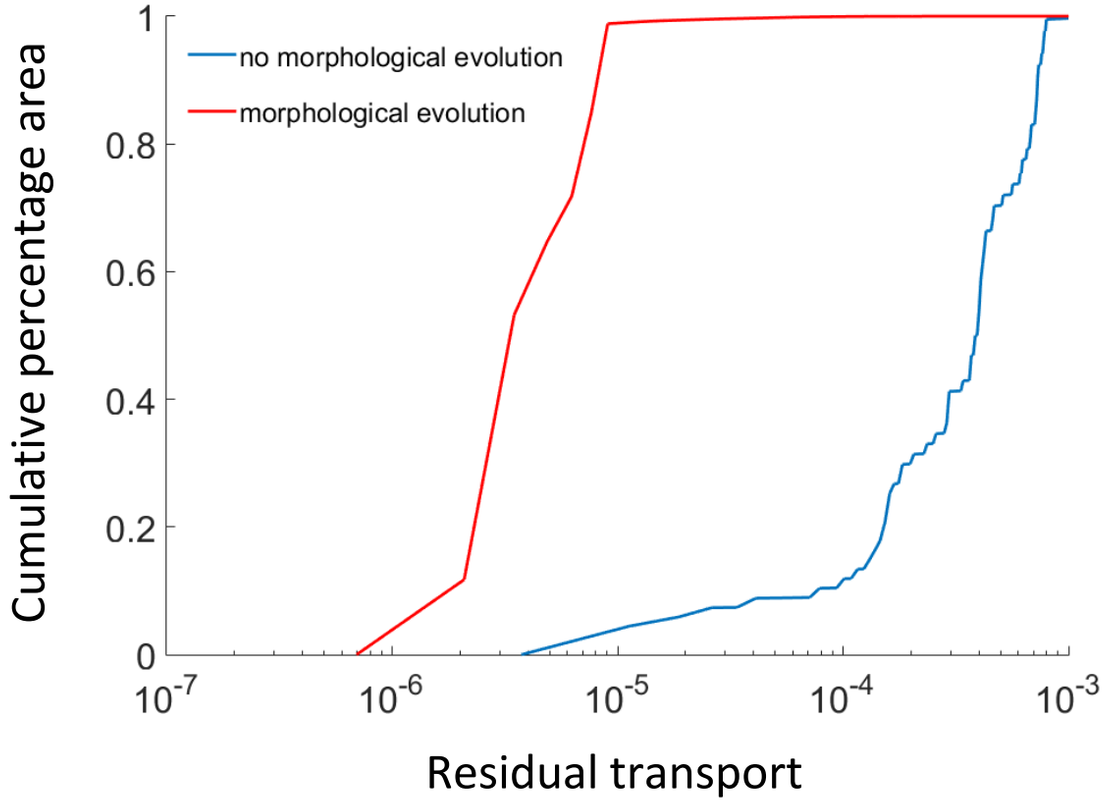
Cumulative percentage area
1
0.8
0.6
0.4
0.2
0
no morphological evolution
morphological evolution
10-7
10-6
10-5
10-4
10-3
Residual transport

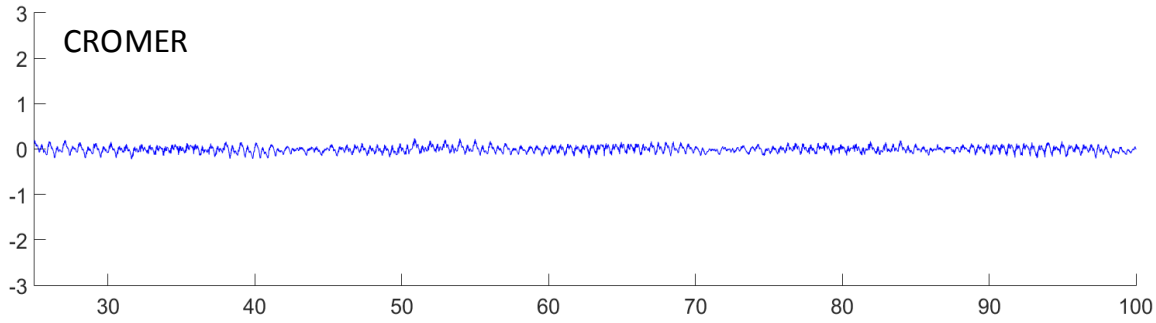
CROMER
3
2
1
0
-1
-2
-3
30
40
50
60
70
80
90
100

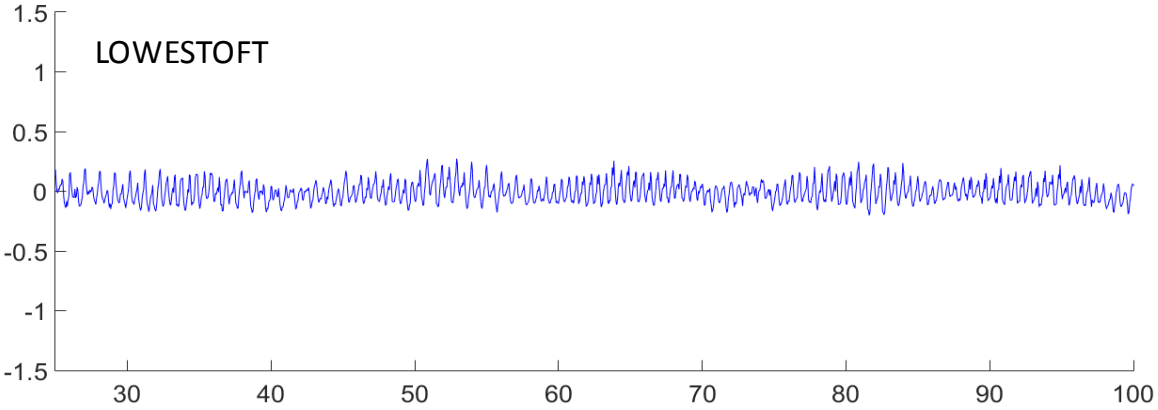
LOWESTOFT
1.5
1
0.5
0
-0.5
-1
-1.5
30
40
50
60
70
80
90
100

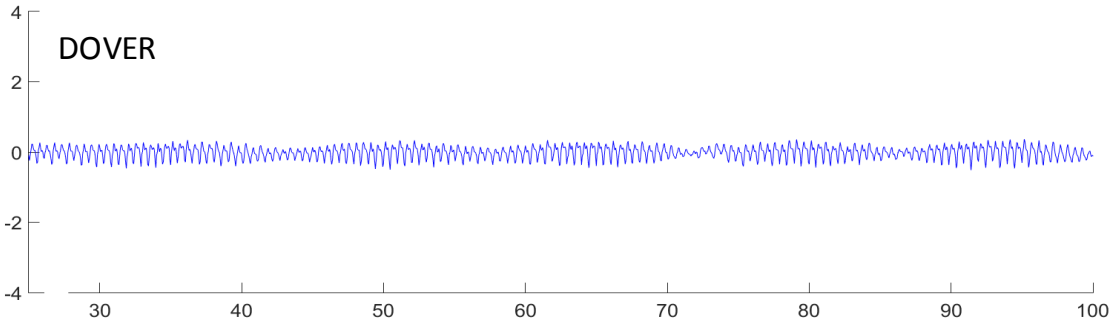
DOVER
4
2
0
-2
-4
30
40
50
60
70
80
90
100

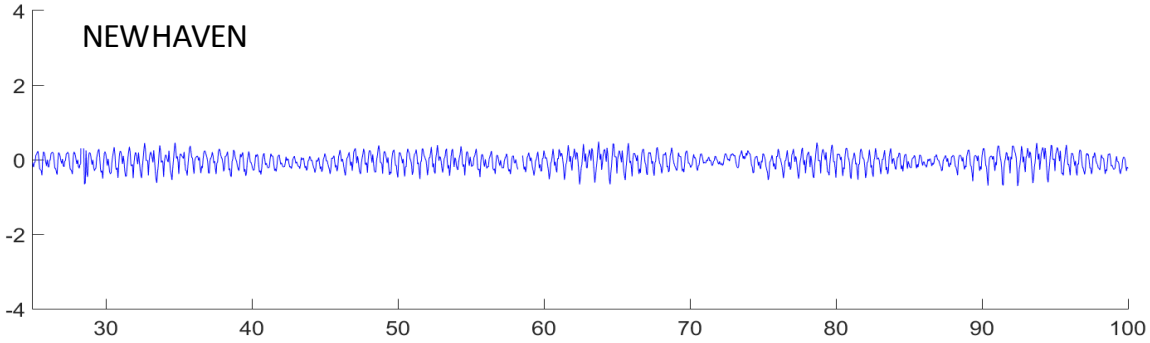
NEWHAVEN
4
2
0
-2
-4
30
40
50
60
70
80
90
100

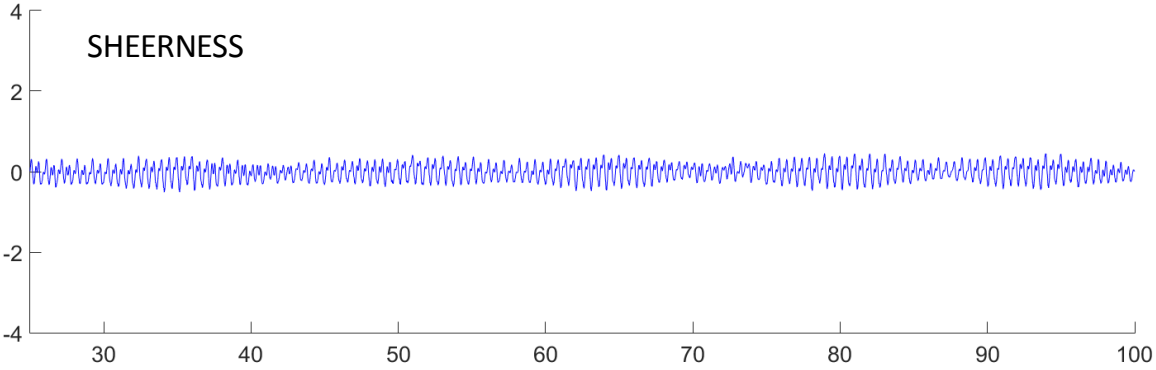
SHEERNESS
4
2
0
-2
-4
30
40
50
60
70
80
90
100

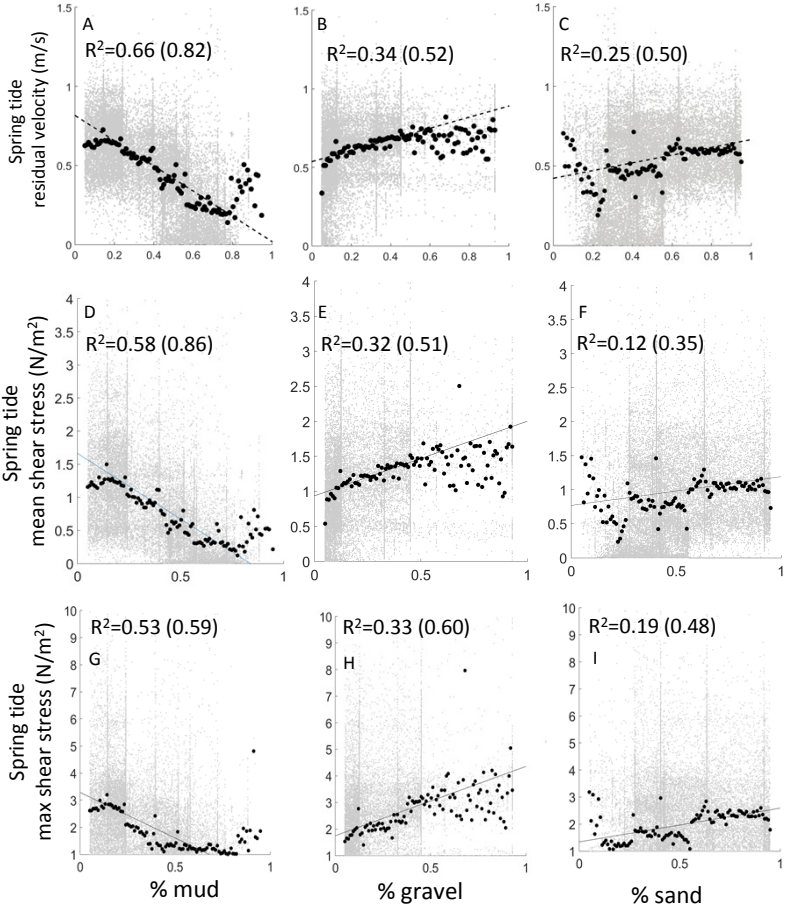
A
R^2=0.66 (0.82)
B
R^2=0.34 (0.52)
C
R^2=0.25 (0.50)
Spring tide residual velocity (m/s)
D
R^2=0.58 (0.86)
E
R^2=0.32 (0.51)
F
R^2=0.12 (0.35)
Spring tide mean shear stress (N/m^2)
G
R^2=0.53 (0.59)
H
R^2=0.33 (0.60)
I
R^2=0.19 (0.48)
Spring tide max shear stress (N/m^2)
% mud
% gravel
% sand

DOVER							
Delft3D	amp (m)	pha (deg)	Buoy data	amp (m)	pha (deg)	Δamp (m)	Δphase (min)
M2	2.239	337.967	M2	2.264	331.573	0.024	1.324
S2	0.691	29.102	S2	0.712	21.615	0.021	1.497
N2	0.394	317.750	N2	0.407	311.366	0.014	1.347
CROMER							
Delft3D	amp (m)	pha (deg)	Buoy data	amp (m)	pha (deg)	Δamp (m)	Δphase (min)
M2	1.600	190.481	M2	1.576	188.255	0.024	0.461
S2	0.531	235.857	S2	0.529	233.070	0.002	0.557
N2	0.310	168.598	N2	0.297	165.574	0.013	0.638
LOWESTOFT							
Delft3D	amp (m)	pha (deg)	Buoy data	amp (m)	pha (deg)	Δamp (m)	Δphase (min)
M2	0.696	252.431	M2	0.678	262.383	0.018	2.060
K1	0.163	319.484	K1	0.153	327.758	0.010	3.300
S2	0.146	281.029	S2	0.149	293.925	0.002	2.579
NEWHAVEN							
Delft3D	amp (m)	pha (deg)	Buoy data	amp (m)	pha (deg)	Δamp (m)	Δphase (min)
M2	2.173	325.350	M2	2.236	319.798	0.064	1.149
S2	0.684	15.691	S2	0.756	18.920	0.072	0.646
N2	0.390	305.033	N2	0.373	297.185	0.018	1.656
SHEERNESS							
Delft3D	amp (m)	pha (deg)	Buoy data	amp (m)	pha (deg)	Δamp (m)	Δphase (min)
M2	2.015	32.418	M2	2.042	39.319	0.027	1.429
S2	0.758	116.586	S2	0.769	124.939	0.011	1.671
N2	0.236	241.771	N2	0.228	255.479	0.008	2.892